Chemical Geology 360–361 (2013) 173–185

Contents lists available at ScienceDirect

Chemical Geology

journal homepage: www.elsevier.com/locate/chemgeo

The influence of buried kimberlite on methane production in overlying sediment, Attawapiskat region, James Bay Lowlands, Ontario

Jamil A. Sader [a,*], Keiko H. Hattori [a], Kerstin Brauneder [a], Stewart M. Hamilton [b]

[a] University of Ottawa, Earth Sciences Department, Ottawa, Ontario K1N 6 N5, Canada
[b] Sedimentary Geoscience Division, Ontario Geological Survey, Sudbury, Ontario P3E 2G9, Canada

ARTICLE INFO

Article history:
Received 11 January 2013
Received in revised form 4 October 2013
Accepted 4 October 2013
Available online 16 October 2013

Editor: David R. Hilton

Keywords:
Methane
Carbon isotopes
Kimberlite
Ultramafic
Water-rock reaction
Peat-bogs

ABSTRACT

Shallow groundwaters were collected over and near buried kimberlites in the Attawapiskat River region of the James Bay Lowlands, Ontario, Canada in order to study the impact kimberlites have on CO_2–CH_4 systematics. Groundwaters collected from boreholes in kimberlites and limestone, and from groundwaters in overlying Tyrell Sea sediment (TSS) were analyzed for $\delta^{13}C_{DIC}$, $\delta^{2}H_{H2O}$, $\delta^{18}O_{H2O}$, dissolved inorganic carbon (DIC), and metal concentrations. Methane gas samples from borehole and TSS groundwaters were analyzed for concentration, $\delta^{13}C_{CH4}$, and $\delta^{2}H_{CH4}$. The CH_4 concentrations and $\Delta^{13}C_{DIC-CH4}$ (isotope separation) values indicate biological carbonate reduction in TSS groundwaters overlying kimberlites. Whereas, $\Delta^{13}C_{DIC-CH4}$ values from TSS groundwaters over limestone and from boreholes within limestone and kimberlite indicate the biological consumption of methane (oxidation). The $\delta^{2}H_{H2O}$ values from TSS over kimberlites are consistent with the variation in $\Delta^{13}C_{DIC-CH4}$, as they are less negative compared to where they should fall on the local meteoric water line, suggesting that methanogens are using lighter $\delta^{2}H_{H2O}$ values to produce CH_4. Biological DIC reduction requires H^+ ions from H_2O to form CH_4. There is evidence in the water geochemistry to support the isotopic results, as the ratio of methane to calculated Fe^{3+} (as amorphous Fe hydroxide), SO_4^{2-}, and $O_{2(aq)}$ is largest in the majority of TSS groundwaters over kimberlites (where $\Delta^{13}C_{DIC-CH4}$ values indicate CH_4 production). Low temperature serpentinization of olivine in kimberlite is not considered for CH_4 production, as redox conditions in kimberlite groundwaters do not support abiogenic methane production. The findings here suggest that kimberlites are indirectly influencing the CO_2–CH_4 system by consuming oxidized ions in the overlying TSS, thereby creating a favorable environment for methane producing bacteria. In contrast, isotopes and geochemistry suggest methane oxidation in areas overlying limestone. The broader implication of this study is that variable lithology underlying sediment cover may impact biological methane production or consumption.

1. Introduction

Methane formation pathways typically occur via reduction (fermentative) of dissolved organic carbon (DOC) or reduction of dissolved inorganic carbon (DIC). These styles of methane formation occur because there are few redox-sensitive ionic species other than carbonate species. Therefore, DOC or DIC reduction commonly proceeds with bacteria as the catalyst (Clymo, 1984; Jakobsen and Postma, 1999; Beer and Blodau, 2007). However, the presence of electron acceptors, such as SO_4^{2-}, Fe^{3+} or dissolved oxygen (DO) can result in the oxidation of methane or the inhibition of its formation (Whiticar and Faber, 1986; Segers, 1988; Miura et al., 1992; Kumaraswamy et al., 2001; Yu et al., 2007).

Previous studies (Reeve et al., 1996; Rejmankova and Post, 1996) have suggested that chemical weathering of soil or rock underlying wetlands can indirectly influence near surface methane flux due to the release of oxidized ions. Additionally, several studies have shown that mineralized zones in crystalline rock emit CH_4 and other hydrocarbons that can be detected at surface (Lovell et al., 1983; McCarthy et al., 1986; Cameron et al., 2004; Sader et al., 2009).

Variable methane concentrations and isotopic compositions may be useful as indicators to pin-point kimberlite bodies that are buried under sequences of sediment. This study investigated the carbon isotope system in Tyrell Sea sediment (TSS), and groundwaters in kimberlite and limestone, over and near known kimberlites in the James Bay Lowlands of northern Ontario, Canada. The goals of this study are to: 1) identify variations in CO_2–CH_4 systematics; 2) investigate controls on the CH_4–CO_2 system in TSS; 3) establish the origin of methane in the Tyrell Sea sediment; and 4) suggest how buried kimberlites influence (either directly through gas migration, or indirectly through changes in redox conditions) the carbon system in overlying sediment.

* Corresponding author at: MMG Limited, Level 26, 1177 West Hastings Street, Vancouver, BC V6E 2K3, Canada.
E-mail address: jamil.sader@mmg.com (J.A. Sader).

0009-2541/$ – see front matter © 2013 Elsevier B.V. All rights reserved.
http://dx.doi.org/10.1016/j.chemgeo.2013.10.007

Redox chemistry, CH_4 and CO_2 concentrations, and $\delta^{13}C$, $\delta^{18}O$, and $\delta^{2}H$ isotopes are used to evaluate CO_2–CH_4 cycling over buried kimberlite and limestone.

2. Location and geology

Kimberlites investigated in this study are located in the James Bay Lowlands in central Canada (Fig. 1), approximately 90 km west of the community of Attawapiskat, Ontario. The kimberlites in this study are also within 15 km of the DeBeers' Victor diamond mine. The kimberlites intruded into Paleozoic sedimentary rocks, predominantly composed of limestone, and underlying basement Archean igneous and metamorphic rocks in the mid-Jurassic (~170 Ma) (Norris, 1993; Webb et al., 2004) (Fig. 2). Host rock to the kimberlites at the bedrock surface is the Upper Attawapiskat Formation limestone. This unit occasionally outcrops in the form of bioherms (coral and skeletal remains) up to 2 m above the surrounding ground surface. All kimberlites in this study subcrop, with the exception of the Zulu kimberlite, which outcrops along its south margin. A thin sheet of till (<1 m) and TSS glaciomarine sediment (2 to 21 m in thickness) overlies the host Upper Attawapiskat Formation limestone and kimberlites (Fig. 2). Although the range in TSS thickness is highly variable, it is generally found to be approximately 13 m thick (DeBeers, pers. comm.).

The region was glaciated during the Quaternary, during which time bedrock surface was eroded and a thin till layer (<1 m) was deposited. The TSS is composed of fine-grained marine sand, silt and clay deposited between 10 and 5 Ka following the end of glaciation when the shoreline of James Bay (known as Tyrell Sea during that period) extended inland approximately 300 km west and southwest of its present location. Isostatic rebound since the retreat of the Laurentide ice sheet in the Attawapiskat region resulted in ground surface elevation increases of 100 to 300 m (Shilts, 1986). The present-day ground surface elevation is 80 to 90 m above sea level. Peat approximately 2.5 to >4.0 m thick overlies the TSS and has been accumulating since the retreat of the Tyrell Sea approximately 5000 years before present. The peat is predominantly composed of sphagnum and becomes progressively more humified with depth (i.e., the sphagnum is increasingly less recognizable below 0.5 m).

The kimberlites consist of abundant olivine macrocrysts, and phenocrysts of ilmenite, garnet, Cr-diopside, phlogopite, and spinel (Kong et al., 1999; Sage, 2000; Armstrong et al., 2004). Kimberlite groundmass mainly consists of carbonate, spinel, and serpentine with

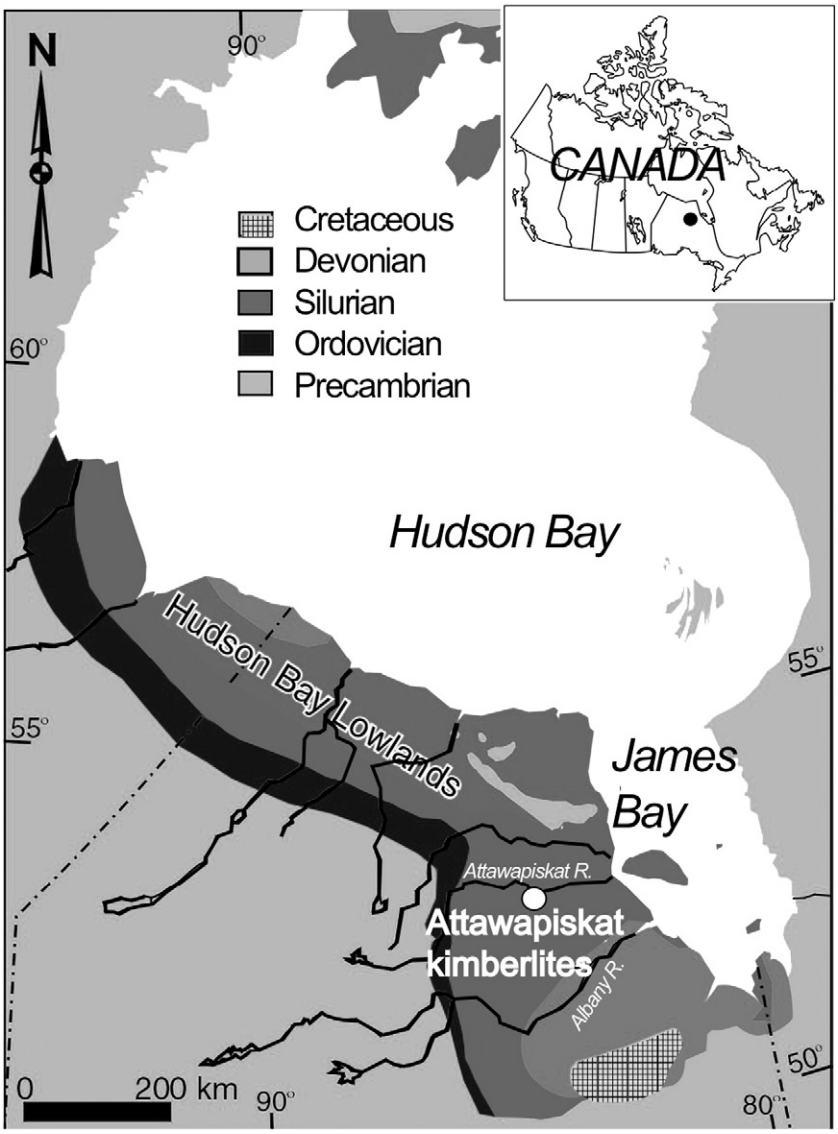

Fig. 1. Regional bedrock geology of the James Bay Lowlands and location of the Attawapiskat kimberlite field in north central Canada. Figure modified from Bellefleur et al. (2005).

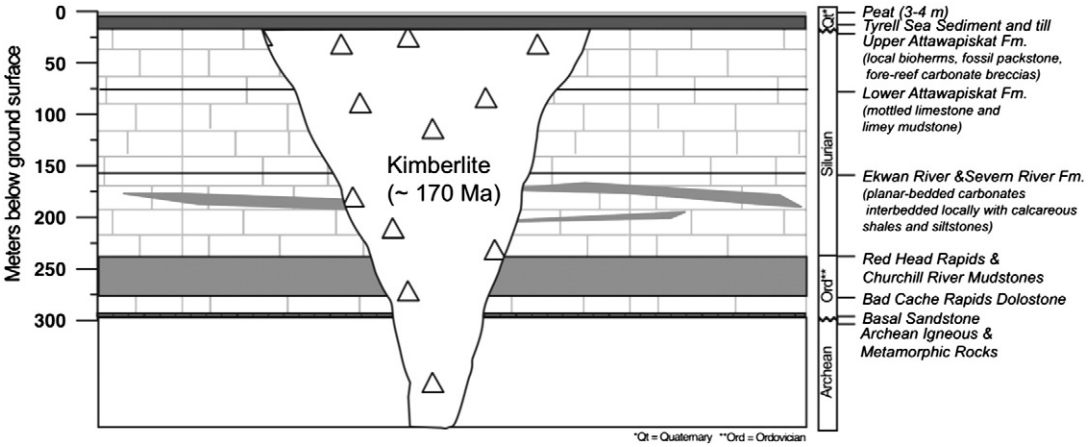

Fig. 2. Schematic vertical section of rocks and sediment of which Attawapiskat kimberlites are emplaced into. Kimberlite and host rocks are overlain by a thin till, Tyrell Sea sediment (12 to 5 Ka), and peat (5 Ka to present). Diagram from (Sader et al., 2011); Geology from Norris (1993).

lesser monticellite, mica, apatite, and perovskite (Kong et al., 1999). All known kimberlites in the Attawapiskat region are either hypabyssal or volcaniclastic (Kong et al., 1999; van Straaten et al., 2009). Kimberlites sampled in this study (Yankee, Zulu, Alpha-1, Golf, and Bravo-1) are altered hypabyssal facies (Sage, 2000).

2.1. Site conditions

The Yankee kimberlite is located between outcropping bioherms southwest and northeast of the kimberlite and the ground surface elevation is slightly lower over the kimberlite compared to immediately surrounding ground surfaces that overly limestone along the transect. The Zulu kimberlite is located east of a lobate raised bog and north of a small bioherm. The site of the Alpha-1 is composed of two bodies (Alpha-1 and Alpha-1 North). The indicator minerals from the two bodies are very similar (Sage, 2000) and suggest they may have been emplaced simultaneously. The ground surface over Alpha-1 and Alpha-1 North has little topographic relief and is a raised bog. The area is bounded by lower elevation fens on the west and east sides of the raised bog. The surface conditions at Bravo-1 kimberlite indicate a slight topographic low and there is standing water up to 30 cm deep at many areas over the kimberlite. In addition to sites of known kimberlites, samples were also collected from the Control site, a location with no known kimberlite in the vicinity (based on geophysical data). This site grades gently towards the Attawapiskat River, approximately 600 m to the north. Ground surface and surface drainage at the Golf kimberlite is similar to that of Zulu (from west to east). The east end of the Golf sampling transects is within 100 m of a bioherm.

3. Methods

3.1. Field procedures

Field sampling and laboratory analytical methods for waters are summarized below from Sader et al. (2011). Monitoring wells were installed into the TSS 0.7 m below the peat/TSS boundary in summer 2007 using stainless steel drive points, iron casings, and low or high-density polyethylene tubing. Three monitoring wells were installed at the Yankee, Zulu, Alpha-1, and Bravo-1 sites; two over each kimberlite and one adjacent to each kimberlite (Fig. 3). One well was installed at the Control site (Fig. 3f). There are no known kimberlites in the region surrounding the Control site. Samples from Yankee, Zulu, Alpha-1, Bravo-1 and Control are denoted by the prefixes of Y, Z, A, B, and C, respectively, and samples collected in the Fall are denoted by the suffix F. Monitoring wells installed during Summer 2007 could not be sampled until Fall 2007, as water levels were slow to recover.

Groundwater samples were collected from existing exploration boreholes (cased through peat, TSS, and till). They are: 1) located approximately 10 m outside and up gradient of the Yankee kimberlite margin within limestone (07-Y-07-7H); 2) south of the center of the Zulu kimberlite (07-Z-07-12C); 3) in the southeast part of Alpha-1 (07-A-BH-06); and 4) near the center of Bravo-1 kimberlite (07-B1-07-08C); (Fig. 3). Borehole groundwaters were collected at a depth of 14 m below ground surface (mbgs). Groundwater was collected from one natural spring (06-Spring) at the Control site.

The pH, oxidation–reduction potential (ORP), electrical conductivity (EC), dissolved oxygen (DO), and temperature was measured on-site for each water sample. A peristaltic pump was used to pump water into a vessel, which contained the pH, ORP, EC, DO and temperature probes. Oxidation reduction potential values have been corrected to the standard hydrogen electrode (SHE) for waters at 10 °C by adding 207 mV to the ORP values, and are reported as Eh. Waters were collected in Nalgene™ high-density polyethylene bottles for cations and anions. Samples for dissolved inorganic carbon (DIC) analysis were collected in 40 mL brown tinted borosilicate bottles with a silicone-poly-tetrafluoroethylene (PTFE) septum cap. An additional PTFE and rubber septum (Chromatographic Specialties Inc.) was inserted underneath the septum cap to prevent DIC loss (silicone is gas-permeable). All water samples were filtered through 0.45 μm Sterivex-HV™ filters (Millipore Corporation).

Methane gas samples were collected using gas diffusion samplers in boreholes and monitoring wells. The gas samplers were constructed of two 10 cm lengths of 9.5 mm (3/8 in.) outside diameter copper tubing with a 10 cm length of gas-permeable silicone tubing fastened in between by wrapping stainless steel wire around the tubing. The two outside ends of the copper tubing (not fastened to the silicone) were crimped and soldered. The reader is directed to Hamilton et al. (2005), Heilweil et al. (2004), Manning and Solomon (2003), Sanford et al. (1996), and Sheldon (2002) for additional descriptions of the diffusion sampler design and its effectiveness at sampling dissolved gas.

The samplers were installed in summer 2007 by suspending them approximately 15 cm above the drive point in monitoring wells (about 3 mbgs) and approximately 14 mbgs in boreholes. During the time between installation and collection, gas diffused into the samplers submerged in groundwater. The gas content in the collectors would then effectively be equal to that of the groundwater. Immediately after retrieval in the Fall of 2007, the open ends of the copper tubing (that were fastened to the silicone tubing) were crimped or clamped, thereby sealing the diffused gas in the copper tubing. The gas samplers were collected from all monitoring wells and boreholes with the exception of the Bravo-1 borehole (07-B1-07-08C).

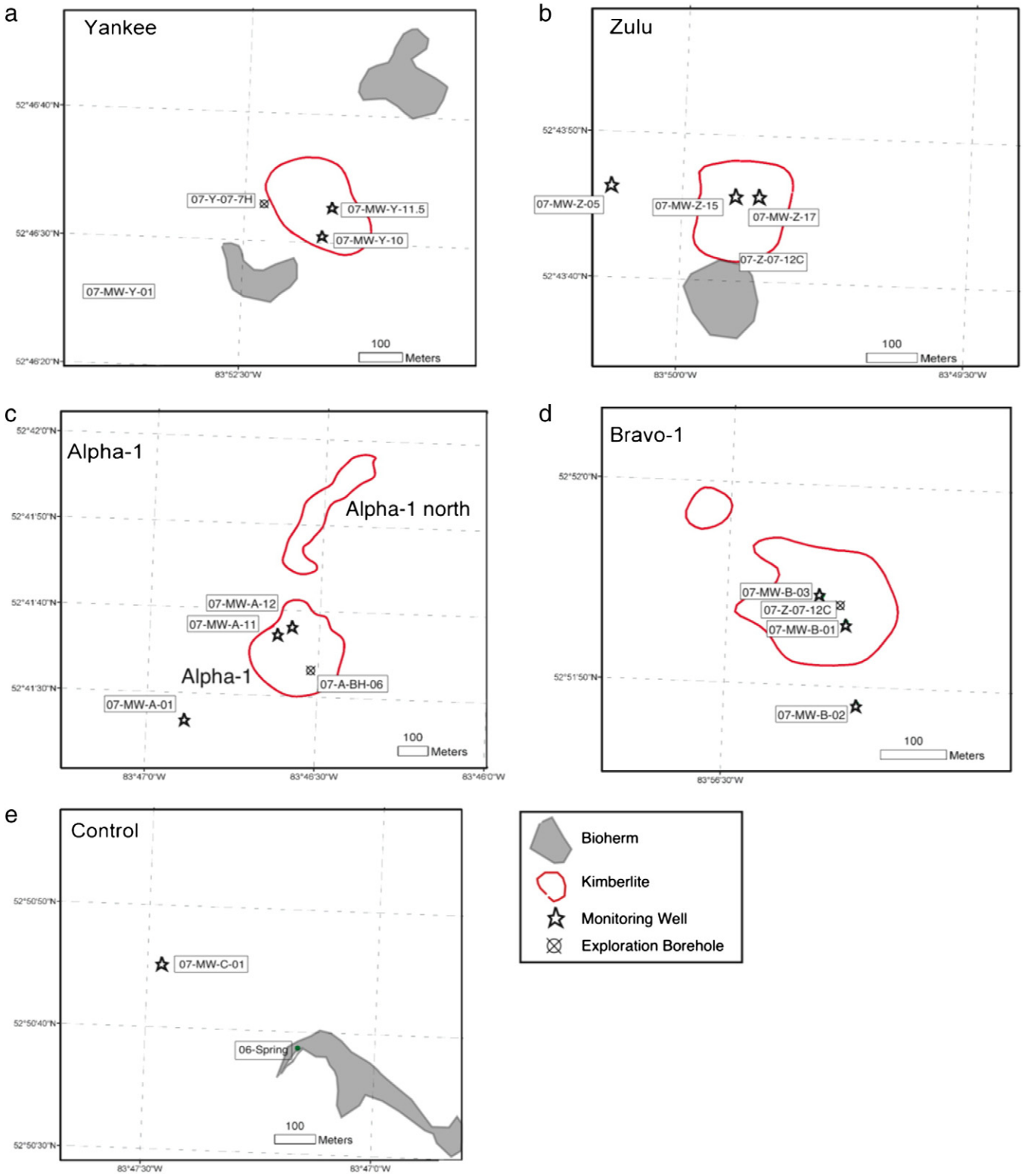

Fig. 3. Location of kimberlites: a) Yankee, b) Zulu, c) Golf, d) Alpha-1, e) Bravo-1, and f) Control Site, boreholes, Tyrell Sea sediment, and peat groundwater sample sites. Areal extent of each kimberlite was determined using geophysical data and exploration drilling by DeBeers Canada.

3.2. Analytical procedures

Waters were analyzed for DIC concentration, and $\delta^{13}C_{DIC}$, $\delta^{2}H_{H2O}$, and $\delta^{18}O_{H2O}$ values at the University of Ottawa G.G. Hatch Stable Isotope Laboratory using a Finnigan-Mat Delta Plus mass spectrometer. The 2σ analytical precision is ±0.002 ppm for DIC, ±0.2‰ for $\delta^{13}C_{DIC}$ values, ±2‰ for $\delta^{2}H_{H2O}$, and ±0.15‰ for $\delta^{18}O_{H2O}$.

The gas from the crimped and sealed copper tubing from the diffusion samplers was extracted by: 1) placing the copper tubing in a vice and crimping the samplers 1.5 cm from one end of the tubing, thereby sealing the tubing in a second spot along its length; 2) then, the tubing was cut between the two crimped segments; 3) a rubber septum coated with silicone grease to provide a gas-tight seal was inserted into the cut end; 4) the space between the septum and the

crimp was flushed with He; 5) the crimp just below the inserted septum was then squeezed in a second vice in order to open it back up (this was possible due to the soft, flexible nature of copper tubing); and 6) lastly, a syringe was used to draw a given volume of gas from the entire length of the tubing. The gas was immediately injected into a gas chromatograph.

Methane gas analyses were conducted at the University of Ottawa G.G. Hatch Laboratory for $\delta^{13}C_{CH4}$ and $\delta^{2}H_{CH4}$ compositions and CH_4 concentrations using a gas chromatograph consisting of a Porabond Q column, connected to a XP Finnigan-MAT IR mass spectrometer. Calibrations were carried out for methane concentration using two international reference standards (NGS1-8559 & NGS2-8560) and one internal reference standard for both C and H isotope analysis. The precisions are 7.7, 3.0, and 2.4% relative standard deviation (RSD) for NGS1-8559, NGS2-8560, and internal standard, respectively. The 2σ analytical precision for $\delta^{13}C_{CH4}$ and $\delta^{2}H_{CH4}$ is ±0.2‰. All $\delta^{13}C$ values are presented in ‰ relative to VPDB and all $\delta^{2}H$ values are relative to VSMOW. Semi-quantitative hydrogen gas content was determined from mass spectrometry data. Quantitative data was not determined, as H standards were not run prior to, and during analysis of gas samples. Therefore, hydrogen gas content is described in terms of the area of well-defined hydrogen peaks along mass spectrometer profiles, and thus these data are considered semi-quantitative.

The molar concentration of methane in the waters was calculated from laboratory-determined methane (in percent concentration) using Henry's Law ($C = P/K$) where: C is the concentration of the gas, P is the pressure, and H is Henry's Law Constant. Note that Henry's Law Constant was calculated based on measured water temperature, and the pressure used in the calculation assumes 1 atm at 0 mbgs plus 0.0967 atm for every meter the gas sampler was installed below the piezometric head at each borehole or monitoring well.

Elemental analyses of groundwaters were conducted at the Ontario Geoscience Laboratories, Ministry of Northern Development and Mines, Sudbury, Canada. Water samples for cations were acidified to 1% concentration prior to analysis using Baseline-grade HNO_3 from Seastar Chemicals. Waters were analyzed for Fe using an inductively coupled plasma mass spectrometer (ICP-MS), and for Na using a Spectro inductively coupled plasma emission spectrometer (ICP-ES). Sulfate and chloride were analyzed using a Dionex ion chromatograph (IC). Analysis of certified reference standard SLRS-4 from the National Research Council of Canada (ICP-MS), FP83MI1 and FP83TE1 (ICP-ES), and internal standards (IC) before, during, and after the run indicated a precision of less than 5% RSD for each metal or species.

4. Results

4.1. Isotopic compositions of TSS, kimberlite, and limestone groundwaters

The concentration of DIC in TSS groundwaters over kimberlite and limestone ranges from 2.7 to 12.8 mmol/L, whereas groundwaters from boreholes in kimberlites and limestone have lower DIC concentrations and range from 1.8 to 6.2 mmol/L. The $\delta^{13}C_{DIC}$ values in TSS groundwaters range from −9.8 to +4.6‰ and have a high degree of variability compared with $\delta^{13}C_{DIC}$ values in groundwaters from kimberlite and limestone, which only varied from −13.7 to −11.4‰ (Table 1). Monitoring wells and borehole groundwaters collected in 2006 have $\delta^{13}C_{DOC}$ values that are consistently −26 ± 1‰ and were similar to values in peat groundwaters (−27 ± 1‰) (Brauneder, 2007).

Methane concentrations in TSS and borehole groundwaters are variable and range from less than detection limit (0.01 mmol/L) to 0.63 mmol/L. These concentrations are below methane saturation at 10 °C for samples collected from monitoring wells and boreholes. Saturation is reached at 1.73 and 2.03 mmol/L for monitoring wells and borehole sample collection depths, respectively. Methane concentrations from boreholes within Zulu and Alpha-1 kimberlites are lower compared to methane concentrations in the TSS over the respective kimberlites. The area of hydrogen peaks along mass spectrometer profiles were compared to the areas of CH_4 peaks, as quantitative data was not available for H_2. Fig. 4 shows H_2 and CH_4 peak areas that are normalized to the volume of gas injected into the GC for each sample. The H_2 content ranges from non-detect (no indication of a profile peak) to significant peak areas that increase with CH_4 peak areas for the majority of the gas samples. However, samples from boreholes within the Zulu and Alpha-1 kimberlites, and from the Zulu borehole appear to contain significant CH_4, but no H_2 (Fig. 4).

The $\delta^{13}C_{CH4}$ values are low (−82.4 to −62.5‰) and the $\delta^{2}H_{CH4}$ values range from −289 to −253‰ (Table 1). $\delta^{13}C_{CH4}$ and $\delta^{2}H_{CH4}$ isotope values in the boreholes within Zulu and Alpha-1, and the borehole in limestone near Yankee do not differ significantly from those samples collected in the TSS. The isotope separation between $\delta^{13}C_{DIC}$ and $\delta^{13}C_{CH4}$ ($\Delta^{13}C_{DIC-CH4}$) versus CH_4 concentration indicates two trends (Fig. 5a). Small decreases in the $\Delta^{13}C_{DIC-CH4}$ values are accompanied by a significant increase in CH_4 concentrations, consistent with CO_2 reduction (Whiticar, 1999). By comparison, $\Delta^{13}C_{DIC-CH4}$ values that are highly variable (range = 55 to 74‰) have sharply decreasing CH_4 concentrations and follow a trend of CH_4 oxidation (Fig. 5a). One sample, 07-Z-07-12C-F (Zulu borehole sample), is the exception, as it has low $\Delta^{13}C_{DIC-CH4}$, but a CH_4 concentrations of 0.31 mmol/L.

Rayleigh fractionation curves were calculated for biological CH_4 production via CO_2 reduction (Eq. (1)) and methane oxidation (Eq. (2)).

$$\delta^{13}C_{CH4(f)} = \delta^{13}C_{DIC(i)} + \varepsilon^{13}C_{DIC-CH4}\cdot(1 + \ln(1-f)) \quad (1)$$

$$\delta^{13}C_{CH4(f)} = \delta^{13}C_{CH4(i)} + \varepsilon^{13}C_{CH4}\cdot(1 + \ln(1-f)) \quad (2)$$

The $\delta^{13}C_{CH4(f)}$ is the resulting $\delta^{13}C_{CH4}$ value after CO_2 reduction. $\delta^{13}C_{DIC(i)}$ is the average initial value in deep groundwaters collected from kimberlites and limestone. The $\varepsilon^{13}C_{DIC-CH4}$ variable represents the isotope fractionation between DIC and CH_4. A value of 71.8‰ was used, as it represents the $\Delta^{13}C_{DIC-CH4}$ isotope separation average for samples that plot along a CO_2 reduction trend in Fig. 5a. It is also similar to the average value of 75‰ for biological CH_4 production via CO_2 reduction in waters (Clark and Fritz, 1997). "*f*" denotes the fraction of methane produced. For Eq. (2), $\delta^{13}C_{CH4(i)}$ is the initial methane value before oxidation; the lowest $\delta^{13}C_{CH4}$ value measured, −82.4‰, was used. The isotope fractionation value of $\varepsilon^{13}C_{CH4}$ (4‰) for residual methane was previously empirically estimated based on CH_4 collected from marine, brackish, and freshwater environments (Whiticar, 1999). The samples that have an isotope separation of approximately 72‰ (Fig. 5a) also plot along a Rayleigh fractionation curve for biological CO_2 reduction (Fig. 5b). Conversely, samples that have an isotope separation < 72‰ plot along the methane oxidation Rayleigh fractionation curve.

A local meteoric water line (LMWL) of $\delta^{2}H_{H2O}$ and $\delta^{18}O_{H2O}$ values in kimberlite, limestone, and TSS groundwaters has a similar slope to that of the Bonner Lake meteoric water line (BLMWL) (Fig. 6). The similarity indicates that Attawapiskat groundwaters are likely meteoric. The BLMWL was generated from precipitation data collected by Birks et al. (2003) at Bonner Lake, Ontario (49.38° N; 82.12° W) and was the closest precipitation monitoring station to the Attawapiskat sample locations. The difference in slope between the two water lines (Fig. 6) is likely due to the fact that Bonner Lake is 400 km south of the study area in a slightly different climatic zone. The magnified inset in Fig. 6 indicates that TSS waters from all but one site over kimberlites, 07-MW-B-01 F (Bravo-1), plot above the BLMWL and display less negative $\delta^{2}H_{H2O}$ values compared with TSS samples collected over limestone. It should be noted that the Bravo-1 sample has CH_4 concentrations that are below the detection limit. Sample 07-MW-A-12F, which has the highest concentration of methane in this study (0.63 mmol/L), also has $\delta^{2}H_{H2O}$ values that deviate the most from the BLMWL. Borehole samples from within Alpha-1 and in limestone near Yankee have isotopic values

Table 1
Geochemical and isotopic values for TSS and borehole waters from Alpha-1, Bravo-1, Control, Yankee, X-Ray, and Zulu kimberlites.

Sample	Kimberlite m	Water type	Location	Latitude degrees	Longitude degrees	Temp °C	pH	Eh mV	EC µS/cm	DO mmol/L	Na µmol/L	Fe^{-} total µmol/L	Fe^{+2} µmol/L	Fe^{+3} µmol/L	SO_4^{2-} µmol/L	Cl^{-} µmol/L	CH µmol/L	$\delta^{13}C_{CH4}$ per mil	$\delta^{2}H_{CH4}$ per mil	DIC mmol/L	$\delta^{13}C_{DIC}$ per mil	$\delta^{2}H_{H2O}$ per mil	$\delta^{18}O_{H2O}$ per mil
07-MWA-01	Alpha-1	TSS	Limestone	52.6907	−83.7810	13.3	7.12	103	481	0.010	139.4	161.8	136.9	24.9	12.5	269.3	na	na	na	5.69	4.28	na	na
07-MW-A-01F	Alpha-1	TSS	Limestone	52.6907	−83.7810	14.5	7.51	263	474	0.044	220.1	97.2	23.3	73.9	4.8	53.2	429.6	−68.22	−265.18	6.37	4.56	−105.70	−14.48
07-MWA-11	Alpha-1	TSS	Kimberlite	52.6938	−83.7769	8.8	7.53	101	524	0.012	1200.9	43.5	23.3	20.2	49.4	120.6	na	na	na	6.49	−3.85	na	na
07-MW-A-11F	Alpha-1	TSS	Kimberlite	52.6938	−83.7769	7.6	6.24	244	377	0.077	2198.0	4.6	0.0	4.6	135.1	290.4	447.1	−70.20	−258.71	5.24	1.53	−94.80	−13.75
07-MWA-12	Alpha-1	TSS	Kimberlite	52.6939	−83.7762	11.5	6.71	209	448	0.208	76.2	85.8	59.1	26.8	5.1	104.2	na	na	na	5.91	0.92	na	na
07-MW-A-12F	Alpha-1	TSS	Kimberlite	52.6939	−83.7762	8.5	7.19	279	248	0.153	56.7	126.5	41.3	85.2	5.1	28.7	632.4	−71.92	−258.60	5.10	−0.04	−63.80	−13.45
07-MW-C-01F	Control	TSS	Limestone	52.8455	−83.7915	16.5	7.44	276	285	0.169	na	na	na	na	na	na	187.7	−70.92	−254.18	6.15	−1.27	−81.60	−11.75
07-MWY-01	Yankee	TSS	Limestone	52.7743	−83.8781	8.4	8.25	60	440	0.019	67.9	15.0	na	na	22.5	bd	na	na	na	na	na	na	na
07-MW-Y-01F	Yankee	TSS	Limestone	52.7743	−83.8781	6.2	6.98	192	410	0.026	45.0	12.0	0.0	12.0	3.6	46.2	358.4	−76.17	−266.35	5.38	−2.22	−99.50	−13.45
07-MWY-10	Yankee	TSS	Kimberlite	52.7752	−83.8725	18.4	9.06	210	409	0.051	81.7	18.7	1.1	17.6	1.7	49.6	na	na	na	4.80	−6.97	na	na
07-MW-Y-10F	Yankee	TSS	Kimberlite	52.7752	−83.8725	5.4	7.40	237	475	0.130	61.8	8.8	0.0	8.8	2.2	37.7	246.6	−76.27	−269.68	5.73	−4.48	na	na
07-MWY-11.5	Yankee	TSS	Kimberlite	52.7759	−83.8721	16.8	8.92	224	407	0.204	110.9	9.4	0.0	9.4	2.8	43.1	na	na	na	4.46	−9.22	na	na
07-MW-Y-11.5F	Yankee	TSS	Kimberlite	52.7759	−83.8721	6.5	8.17	212	411	0.090	96.8	10.5	0.0	10.5	2.8	39.2	116.1	−82.42	−289.21	4.70	−9.83	−104.80	−15.22
07-MWZ-05	Zulu	TSS	Limestone	52.7298	−83.8354	16.4	6.57	102	479	0.000	155.7	35.5	13.5	22.0	2.1	bd	na	na	na	10.50	−7.75	na	na
07-MW-Z-05F	Zulu	TSS	Limestone	52.7298	−83.8354	16.4	7.67	175	304	0.061	359.2	4.0	0.0	4.0	10.1	60.6	11.3	−62.47	−253.02	2.67	−5.60	na	na
07-MWZ-15	Zulu	TSS	Kimberlite	52.7296	−83.8316	na	na	na	na	0.000	54.1	107.4	na	na	1.7	37.7	na	na	na	6.51	−2.57	na	na
07-MW-Z-15F	Zulu	TSS	Kimberlite	52.7296	−83.8316	7.1	7.24	281	440	0.085	38.6	105.0	31.2	73.8	0.4	26.2	153.1	−68.00	−275.70	6.99	−5.21	−100.80	−14.77
07-MW-Z-17F	Zulu	TSS	Kimberlite	52.7296	−83.8309	6.5	7.66	241	874	0.018	1658.2	2.0	0.0	2.0	12.9	105.4	421.3	−68.63	−261.35	12.77	3.22	−99.20	−15.04
07-MW-B-01F	Bravo-1	TSS	Kimberlite	52.8647	−83.9390	9.6	6.77	341	434	0.213	130.5	2.3	0.0	2.3	5.1	74.1	bd	bd	bd	5.12	−5.38	−92.60	−11.95
07-MW-B-02F	Bravo-1	TSS	Limestone	52.8636	−83.9387	6.2	6.71	306	977	0.240	669.6	1.9	0.0	1.9	13.3	249.3	bd	bd	bd	10.83	3.20	na	na
07-MW-B-03F	Bravo-1	TSS	Kimberlite	52.8651	−83.9395	15.1	7.54	303	600	0.059	194.1	0.8	0.0	0.8	5.9	69.3	bd	bd	bd	5.85	−3.48	na	na
07-B1-07-08C-F	Bravo-1	Borehole	Kimberlite	52.8649	−83.9393	9.6	8.55	226	597	0.078	323.6	1.3	0.0	1.3	2.5	169.0	na	na	na	6.17	−7.16	−97.60	−12.54
07-X-07-014C	X-Ray	Borehole	Kimberlite	52.7960	−83.8537	9.0	7.76	23	198	0.000	36.2	5.4	0.0	5.4	7.0	14.1	na	na	na	3.16	−2.03	na	na
07-Z-07-12C	Zulu	Borehole	Kimberlite	52.7290	−83.8317	12.4	7.51	68	945	0.000	51.0	221.6	214.6	6.9	4.5	28.2	na	na	na	4.12	−10.27	na	na
07-Z-07-12C-F	Zulu	Borehole	Kimberlite	52.7290	−83.8317	16.9	8.04	136	247	0.040	43.5	229.2	221.3	7.9	0.4	21.7	71.0	−75.94	−272.93	4.41	−11.43	−65.90	−10.86
07-Y-07-7H	Yankee	Borehole	Kimberlite	52.7756	−83.8737	7.5	8.06	−4	377	0.000	5120.3	8.0	0.9	7.1	136.4	4459.4	na	na	na	6.34	−12.60	na	na
07-Y-07-7H-F	Yankee	Borehole	Kimberlite	52.7756	−83.8737	16.9	7.29	95	na	0.039	416.2	24.5	7.2	17.3	40.8	422.0	311.8	−73.02	−261.24	1.94	−12.33	−110.80	−15.04
07-A-BH-06	Alpha-1	Borehole	Kimberlite	52.6922	−83.7752	9.1	7.21	272	na	na	842.0	66.2	26.8	39.3	11.6	182.8	10.0	−68.66	−287.10	1.81	−13.70	na	na

na = Not analyzed.
bd = Below detection.

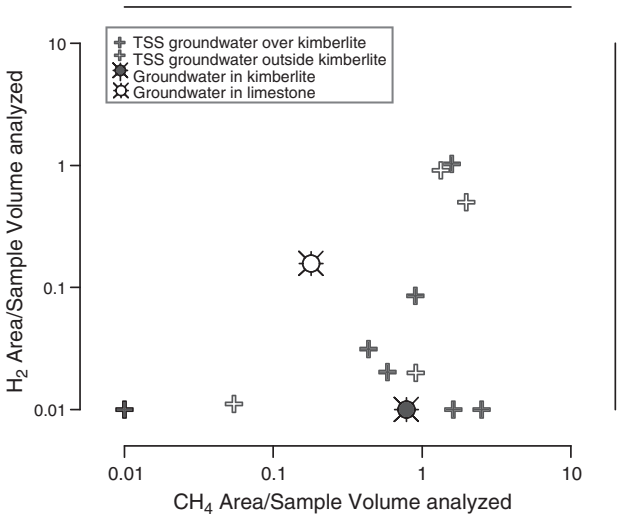

Fig. 4. A plot of CH_4 versus H_2 for TSS and monitoring well gas samples. The diagram indicates that for approximately half of the samples, H_2 increases with increasing CH_4 concentrations. However, there are a number of samples that demonstrate high CH_4 concentrations, but H_2 is below detection.

that plot on or slightly below the BLMWL. However, the borehole sample from the Zulu kimberlite plots above the BLMWL.

The plot of δ^2H_{CH4} and δ^2H_{H2O} (Fig. 7) indicates that origin of CH_4 measured in this study, which is either forming or being oxidized, was almost entirely derived from carbonate reduction. Samples from the Zulu kimberlite borehole, and TSS samples 07-MW-A-12A and 07-MW-Y-11.5 F (over kimberlites) appear to have a contribution from methyl fermentation and plot on or near an 80% carbonate reduction, 20% methyl fermentation slope (Whiticar, 1999). During bacterial CO_2 reduction, bacteria will utilize the H^+ in water during methane formation. Fractionation between δ^2H_{H2O} and δ^2H_{CH4} during bacterial DIC reduction is consistently $-160 \pm 10‰$ (Schoell, 1980; Whiticar et al., 1986; Whiticar, 1999) and is demonstrated through the following linear relationship (Eq. (3)):

$$\delta^2H_{CH4} = \delta^2H_{H2O} - 160‰ \quad (3)$$

Conversely, methane from methyl fermentation only uses one H^+ from H_2O and three H^+ ions derived from organic acid, and therefore the process is dominantly reliant on the δ^2H values of the organic acids rather than water (Whiticar et al., 1986). Had the majority of H^+ been derived through methyl fermentation for these samples, they would likely comprise more negative δ^2H_{CH4} values of approximately -380 to $-390‰$. The samples would then plot nearer to the %C:%M = 0:100 line (Fig. 7).

4.2. Geochemical compositions of TSS, kimberlite, and limestone groundwaters

The pH values in TSS, kimberlite, and limestone groundwaters are circumneutral to slightly alkaline (7.1 to 9.1 with an average of 7.5). The Eh values in TSS groundwaters (average 217 mV) are typically more elevated compared with Eh values in boreholes from kimberlites (average = 90 mV) (Table 1). Sulfate concentrations in borehole and TSS groundwaters are low. The mean, maximum, and minimum SO_4^{2-} concentrations are 14.7 μmol/L, 135 μmol/L, and 0.4 μmol/L (detection limit), respectively. In contrast, Fe concentrations in TSS and borehole groundwaters were typically 4 to 5 times greater than SO_4^{2-} concentrations (Table 1). The speciation of Fe^{2+} and Fe^{3+} was calculated using Geochemists WorkBench (Bethke, 2002) and varied from dominantly ferric to dominantly ferrous Fe in all groundwaters.

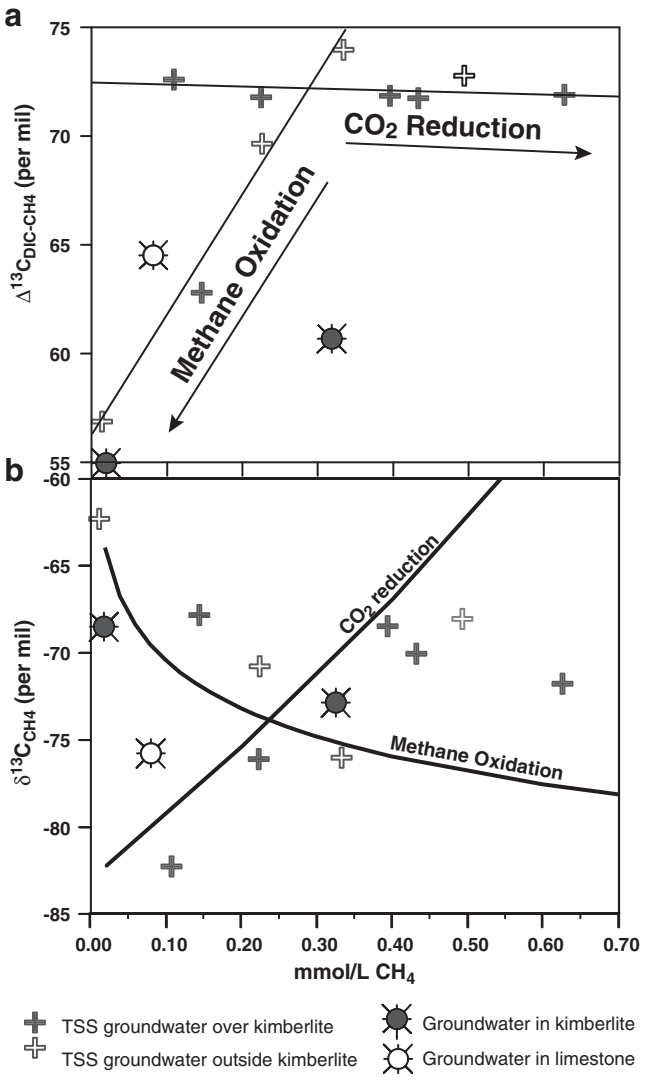

Fig. 5. a) A plot of $\delta^{13}C_{DIC-CH4}$ values versus methane content for monitoring wells and boreholes. The small decrease in isotope separation with increase in methane concentrations suggests methane production. Conversely, the sharp decline in isotope separation with decreases in methane concentrations suggests methane oxidation. b) Plot of methane content versus $\delta^{13}C_{CH4}$. Thick black lines indicate trends for Rayleigh fractionation for $\delta^{13}C_{CH4}$ during CO_2 reduction (Eq. (1)) and methane oxidation (Eq. (2)). Samples that plot along the Rayleigh fractionation curve for CO_2 reduction also display isotope separation of approximately 72‰. Samples less than 72‰ plot along the methane oxidation Rayleigh fractionation curve. Methane saturation is 2.03 mmol/L CH_4 at sampling pressure and temperature conditions.

5. Discussion

5.1. Geochemical influences on in situ methane production and oxidation

Variations in concentrations of oxidized ions such as SO_4^{2-}, Fe^{3+}, and $O_{2(aq)}$ relative to CH_4 are likely controlling in situ formation or oxidation of CH_4. Ratios of CH_4/Fe^{3+}, CH_4/SO_4^{2-}, and $CH_4/O_{2(aq)}$ remain low (<10, 5, and 1, respectively) where the $\Delta^{13}C_{DIC-CH4}$ values are <72‰ (Fig. 8). These low ratios are commonly spatially associated with TSS samples collected over limestone.

Where $\Delta^{13}C_{DIC-CH4}$ values are approximately 72‰ (mostly samples from TSS over kimberlites), the molar ratios of CH_4/Fe^{3+}, CH_4/SO_4^{2-}, and $CH_4/O_{2(aq)}$ increase up to 400 (Fig. 8). This pattern suggests that the consistent and high $\Delta^{13}C_{DIC-CH4}$ values (indicative of CH_4 production) are due to decreases in concentrations of oxidized ions, thereby making conditions more favorable for the reduction of DIC. The migration of reduced ions and kimberlite pathfinder metals

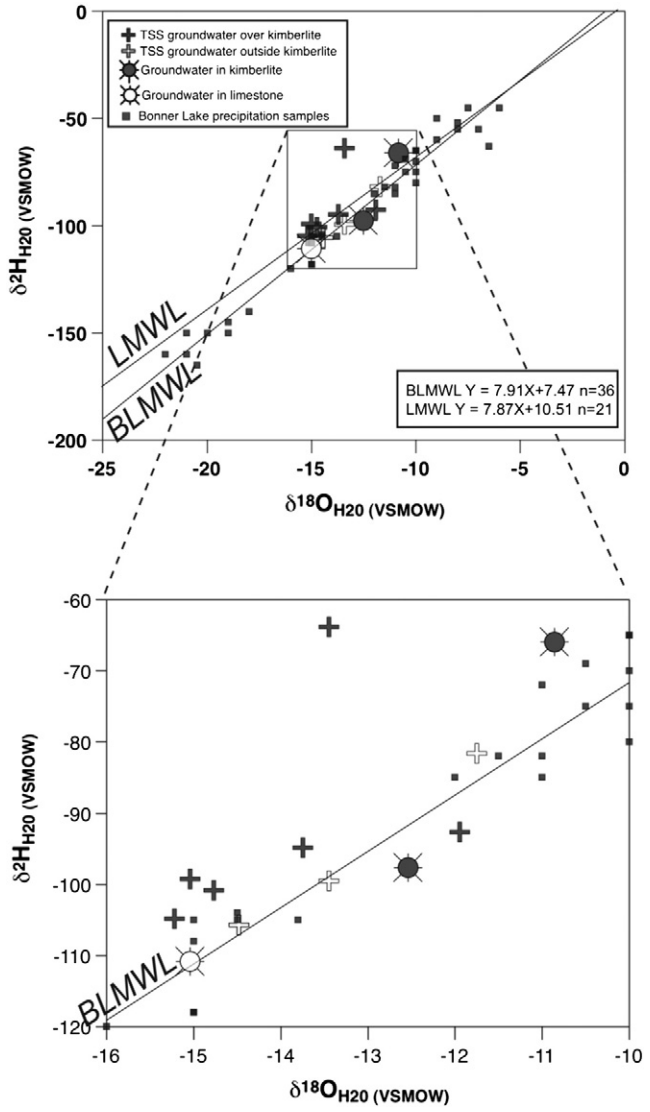

Fig. 6. The δ^2H_{H2O} and $\delta^{18}O_{H2O}$ values from kimberlite, limestone, and TSS groundwaters plot on a local water line (LMWL). The slope of the LMWL is similar to the Bonner Lake meteoric water line (BLMWL) based on precipitation data from Bonner Lake, Ontario (49.38° N; 82.12° W). The expanded plot indicates that the majority of samples collected from the TSS over kimberlite plot above the LMWL and have heavier δ^2H_{H2O} values. The similarity of the two slopes indicates that groundwaters in this study are meteoric. Data for construction of the BLMWL obtained from Birks et al. (2003).

upwards from kimberlites to TSS via upward groundwater movement has been suggested (Sader et al., 2011). Most groundwaters over limestone and in boreholes have low ratios of CH_4/Fe^{3+}, CH_4/SO_4^{2-}, and $CH_4/O_{2(aq)}$ (Fig. 8). These low ratios suggest that conditions are favorable for CH_4 oxidation. Additionally, the samples with low CH_4/Fe^{3+}, CH_4/SO_4^{2-}, and $CH_4/O_{2(aq)}$ ratios are the same ones that plot along a trend of biological methane oxidation (sharp decreases in methane concentrations with decreases in the $\Delta^{13}C_{DIC-CH4}$ values; Fig. 5a). These relationships suggest that methane oxidation may be due to anaerobic or aerobic methanotrophs.

The reduction of DIC results in lower energy yields for bacteria compared to bacterial reduction of SO_4^{2-}, Fe^{3+}, or $O_{2(aq)}$. Therefore, where Fe^{3+}, SO_4^{2-}, and $O_{2(aq)}$ concentrations are elevated relative to CH_4, the oxidized ions likely inhibit or suppress methanogenic bacteria in favor of methanotrophs due to competitive effects (Whiticar and Faber, 1986; Segers, 1988; Achtnich et al., 1995). However, in the absence of oxidized ions such as SO_4^{2-}, Fe^{3+}, and $O_{2(aq)}$ methanogens are commonly more predominant (Segers, 1988). The occurrence of CH_4 in low concentrations (<0.2 mmol/L), which exist in the presence of elevated oxidized ions and represent samples along the methane oxidation trend (Fig. 5a), may represent residual methane that is not oxidized by bacteria. Methane concentrations <0.15 mmol/L have been documented to commonly coexist with Fe^{3+} and SO_4^{2-} reducing bacteria (Martens and Berner, 1977; Jakobsen and Postma, 1999). Whiticar and Faber (1986) suggest that this coexistence is attributed to CH_4 concentrations that are too low for methanotrophic bacteria to utilize.

5.2. CH_4 isotope systematics and biological DIC reduction

5.2.1. $\delta^{13}C_{CH4}$ and $\delta^{13}C_{DIC}$ systematics

The consistent $\Delta^{13}C_{DIC-CH4}$ values of approximately 72‰ for almost all TSS groundwaters over kimberlites, coupled with increases in CH_4 concentrations, suggest CH_4 production via biological reduction of DIC (Fig. 5a). The high and consistent $\Delta^{13}C_{DIC-CH4}$ values typically indicate bacterial DIC reduction because the $\delta^{13}C_{DIC}$ values become higher at approximately the same rate that $\delta^{13}C_{CH4}$ values become equally higher in a closed system (no gains or losses of C or H in the system from outside sources) (Whiticar, 1999). Bacterial CO_2 reduction is further suggested because the same groundwaters that have $\Delta^{13}C_{DIC-CH4}$ of approximately 72‰ plot near a trend of Rayleigh fractionation for CO_2 reduction (Fig. 5b).

For most TSS groundwater samples outside kimberlite (over limestone), and deeper groundwaters from kimberlite and limestone, a sharp decrease in $\Delta^{13}C_{DIC-CH4}$ values is accompanied by a decrease in CH_4 concentrations (Fig. 5a). This trend suggests that CH_4 is most likely being consumed by methanotrophic bacteria, and is characteristic of bacterial methane oxidation in both freshwater and marine environments (Whiticar, 1999). The decrease in $\Delta^{13}C_{DIC-CH4}$ values is due to the preferential use of ^{12}C by methanotrophic bacteria, thereby resulting in higher $\delta^{13}C_{CH4}$ values as CH_4 concentrations decrease along the Rayleigh fractionation trend (Fig. 5b).

The addition of DIC with low values (closer to that of $\delta^{13}C_{CH4}$) could also result in variable (and lower) $\Delta^{13}C_{DIC-CH4}$ values, and could indicate methane oxidation, as shown in Fig. 5a. However, samples that plot along the trend of CH_4 oxidation in the plot of $\Delta^{13}C_{DIC-CH4}$ versus CH_4 concentration are the same samples that plot along the Rayleigh fractionation trend of CH_4 oxidation in Fig. 5b. As calculation of the Rayleigh fractionation trend for methane oxidation does not involve $\delta^{13}C_{DIC}$ values, low $\Delta^{13}C_{DIC-CH4}$ associated with inputs of isotopically light DIC is not likely.

Sample 07-MW-Z-15, collected over the Zulu kimberlite, is the only monitoring well groundwater sample collected over kimberlite where methane oxidation is indicated. This sample may have been contaminated by peat pore water close to the peat/TSS boundary, as the monitoring well drive point could not be fully driven into the marine sediment below the peat. Low Na and Cl concentrations in the water compared to groundwater samples from other monitoring wells at Zulu are consistent with a contribution from ombrotrophic peat groundwater (Sader et al., 2011).

The only sample that does not fit a trend of CH_4 oxidation or production in Fig. 5a & b is 07-Z-07-12C-F (groundwater from Zulu kimberlite borehole). Rather, this sample has a low $\Delta^{13}C_{DIC-CH4}$ value of 60.7‰, but the methane concentration is high (0.31 mmol/L) and the sample plots near the intersection of the Rayleigh fractionation trends for CO_2 reduction and methane oxidation (Fig. 5a & b). There are two possible explanations as to why the data for sample 07-Z-07-12C-F are ambiguous compared with other samples. It is possible that the sample represents mixing between methane from two different sources. Fig. 7 indicates that as much as 20% of this methane sample was produced via methyl fermentation. The addition of methane from low-temperature serpentinization of olivine in kimberlite could also potentially result in lower $\Delta^{13}C_{DIC-CH4}$ and $\delta^{13}C_{CH4}$ values. Methane is commonly favored to form through the process of low temperature serpentinization of olivine in ultramafic rocks (Barnes et al., 1972;

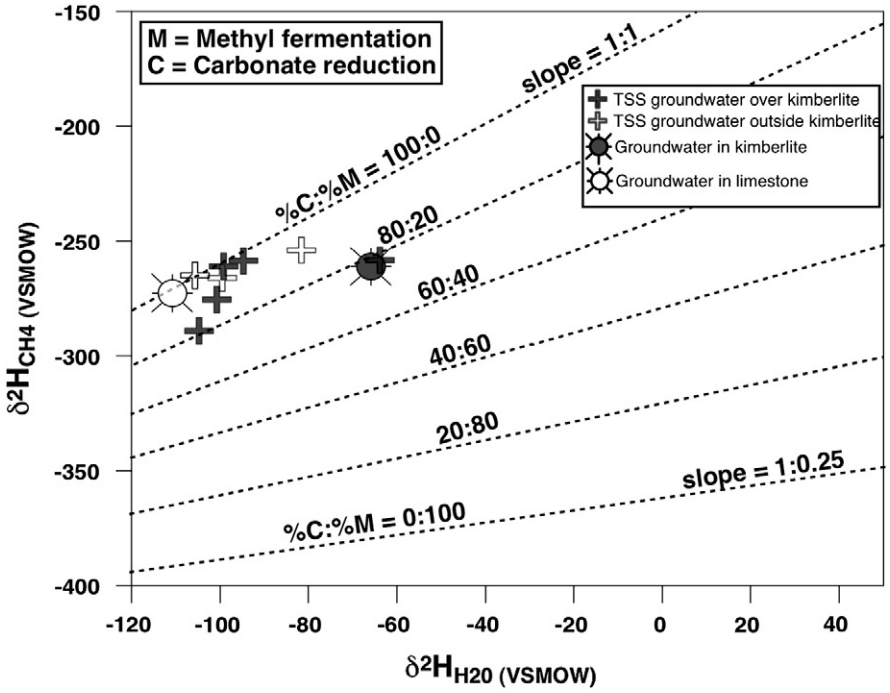

Fig. 7. The δ^2H_{CH4} and δ^2H_{H2O} values in groundwaters from TSS, limestone, and kimberlite plot near the 1:1 slope, indicating a biological CO_2 reduction origin of the methane. The ratios of carbonate reduction versus methyl fermentation and slopes are from Whiticar (1999).

Abrajano et al., 1988; Fritz et al., 1992; Sader et al., 2007a) (Eq. (4)). However, a serpentinization pathway is

$$15(Mg, Fe)_2SiO_4(FO_{90}) + 20H_2O + 0.25CO_2 \rightarrow$$

$$Fe_3O_4 + 7.5Mg_3Si_2O_5(OH)_4 + 4.5Mg(OH)_2 + 0.25CH_4 \quad (4)$$

not suggested for this study, and therefore the production of abiogenic CH_4 is not likely. Abiogenic CH_4 typically forms under redox conditions that are significantly lower ($Eh \leq -200$ mV at pH values of 6 to 7) than which occurs in the kimberlites in this study. The Eh values observed in Attawapiskat kimberlite groundwaters (this study) range from 23 to 272 mV. Sader et al. (2007a) suggested that kimberlite groundwaters that had bicarbonate alkalinity and pH only 1 to 2 units greater than 7 and oxidizing Eh values may be a result of short groundwater residence time within kimberlites. Low residence time could result in less water–kimberlite (olivine) interactions.

The $\delta^{13}C_{CH4}$ values in samples from kimberlite do not support an abiogenic source, as the values are low (−73 and −68.7‰ at 07-Z-07-12C-F and 07-A-BH-06, respectively). The $\delta^{13}C_{CH4}$ values typically associated with serpentinization reactions and abiogenic methane formation range between −10 and −20‰ (Abrajano et al., 1988; Fritz et al., 1992; Proskurowski et al., 2008).

5.2.2. $\delta^{18}O_{H2O}$ and δ^2H_{H2O} evidence for CH_4 production

The plot of $\delta^{18}O_{H2O}$ and δ^2H_{H2O} (Fig. 6) provides further evidence for bacterial DIC reduction processes in TSS samples collected over kimberlites. All but one TSS sample collected over kimberlites, and the borehole within the Zulu kimberlite (07-Z-7-12C) has δ^2H_{H2O} values that plot above the BLMWL (less negative) (Fig. 6). Conversely, samples from TSS over limestone or from the Yankee borehole within limestone plot closer to or below the BLMWL. The less negative δ^2H_{H2O} associated with TSS samples over kimberlites suggests Rayleigh fractionation of H isotopes as methane is produced. During the biological reduction of DIC, the methane that is produced derives all its hydrogen atoms from water (Whiticar, 1999). Methanogenic bacteria will preferentially use lighter H_{H2O}, thereby fractionating to less negative δ^2H_{H2O} values. The effect of this process has been shown in studies where CH_4 is being produced through the biological reduction of DIC (Clark and Fritz, 1997; Siegel et al., 2001).

Isotopic mass balance calculations were conducted to estimate the CH_4 that would be produced based on the deviation of δ^2H_{H2O} towards less negative values (samples that plot above the BLMWL) in Fig. 6. The fractionation equation used is:

$$\delta^2_f H_{H2O} = \delta^2_o H_{H2O} + 10^3 \cdot (\alpha^2 H_{H2O\text{-}CH4} - 1) \ln f$$

where $\delta^2_f H_{H2O}$ is the measured isotopic value and $\delta^2_o H_{H2O}$ is the value if it is plotted along the BLMWL (no fractionation). The variable $\alpha^2H_{H2O\text{–}CH4}$ is 2.26, and was empirically determined by Bottinga (1969), and "*f*" is the fraction of CH_4 produced per liter H_2O. The calculated CH_4 concentrations based on the fractionation of δ^2H_{H2O} to more positive values from the BLMWL in Fig. 6 is on the order of mol/L of CH_4 and is roughly 3 orders of magnitude higher than the measured CH_4 concentrations (Fig. 9). However, for samples collected over kimberlites and from the Zulu kimberlite, there is a linear correlation ($r = 0.80$) between the measured and calculated methane concentrations (increasing measured CH_4 with increasing calculated CH_4). This correlation suggests that the production of methane did result in a positive shift in δ^2H_{H2O} values. However, the 3 orders of magnitude difference between calculated and measured methane concentrations may be related to methane loss over time due to diffusion or ebullation of gas from formation waters. Siegel et al. (2001) indicated that calculated methane production (based on δ^2H_{H2O} values, which plotted above the LMWL for sites from a bog in Minnesota) was approximately an order of magnitude greater than measured methane. In that study it was suggested that loss occurred due to methane migration or their gas samplers did not collect a portion of gas dissolved in groundwater. Although methane was observed in groundwaters from TSS over limestone they do not demonstrate a correlation with the calculated values (Fig. 9). This lack of correlation may indicate that water carrying dissolved methane migrated to TSS and underwent oxidation — the source potentially being overlying peat groundwaters containing dissolved methane.

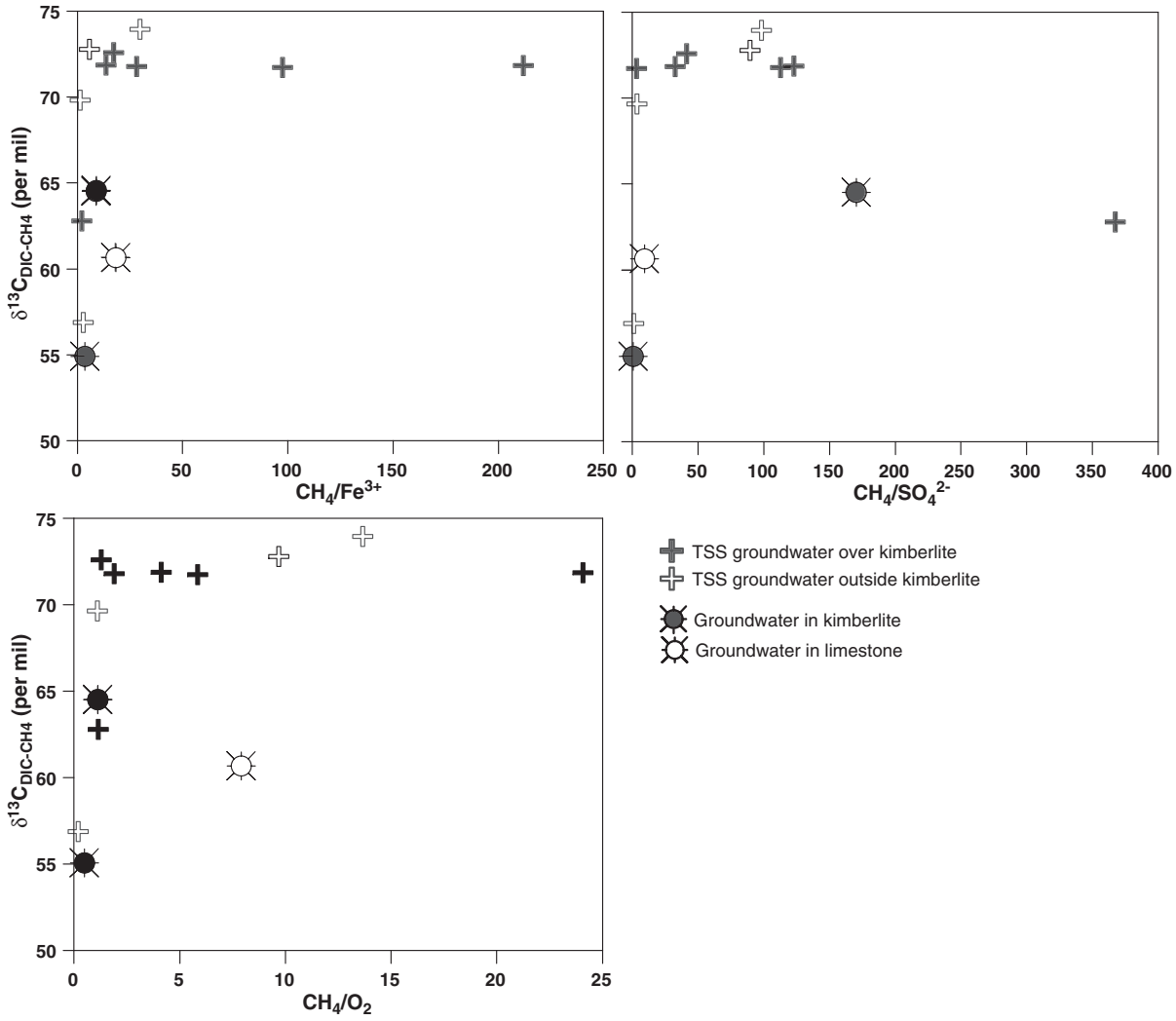

Fig. 8. Plots of low CH_4/Fe^{3+} and CH_4/SO_4^{2-} ratios coupled with low $\delta^{13}C_{DIC-CH4}$ suggest that methane oxidation is occurring due to the high concentrations of oxidized ions. Conversely, samples with high CH_4/Fe^{3+} and CH_4/SO_4^{2-} and high $\delta^{13}C_{DIC-CH4}$ are dominantly those collected in TSS over kimberlites and suggests that kimberlites may be consuming oxidized ions. This may provide bacteria with more suitable conditions for CO_2 reduction. All ratios are molar ratios.

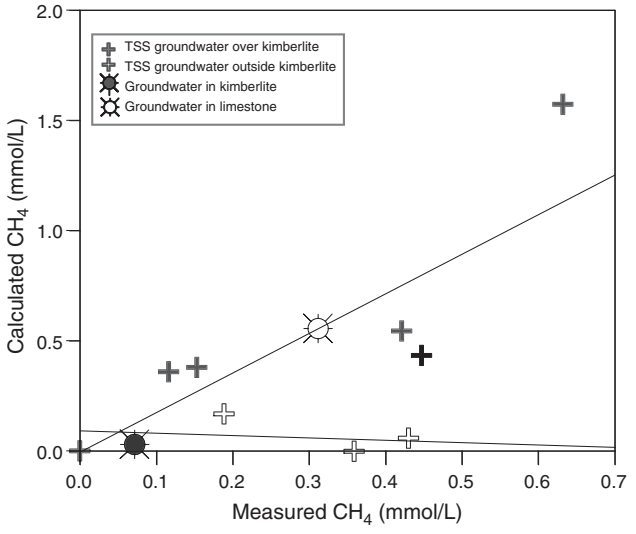

Fig. 9. The calculated versus measured CH_4 for groundwater samples from TSS and boreholes. Calculations for CH_4 are based on how much heavier δ^2H_{H2O} values are compared with the BLMWL (see Fig. 6). Note that the calculated methane is approximately 3 orders of magnitude greater than measured methane.

5.3. Sources of H_2 for methane production

In order to reduce DIC and produce CH_4, methanogenic bacteria require H_2 to function as an electron donor. Appreciable abiogenic H_2 production by low-temperature serpentinization of olivine is unlikely, given that the redox conditions do not favor the hydrolysis of H_2O. Additionally, abiogenic H_2 produced by low temperature serpentinization, as noted in Kirkland Lake kimberlites (Sader et al., 2007b), typically has low δ^2H_{H2} values ranging from −599 to −800‰ (Abrajano et al., 1988; Fritz et al., 1992; Sader et al., 2007b). If methanogenic bacteria had utilized H_2 from this source much lower δ^2H_{CH4} values would be expected to be present. Instead, the decomposition of organic material and the production of H_2 is the most likely source and may be utilized by bacteria to reduce DIC. Environments with high concentrations of organics are commonly major sources for H_2 (Clark and Fritz, 1997). Although CH_4 and H_2 do not correlate positively for some gas samples (Fig. 4), it is reasonable to suspect that H_2 is available and is being utilized to reduce DIC. Measureable H_2 concentrations are not always indicative of a dominant electron accepting process (Jakobsen et al., 1998; Jakobsen and Postma, 1999; Hansen et al., 2001). In each of these studies, the calculated energy yield was too low for the biological production of methane (low H_2 concentrations), yet the studies show strong evidence for in situ CH_4 formation.

5.4. Origin of methane outside kimberlites

The source of CH_4 in TSS outside kimberlites and in limestone in this study is difficult to delineate. It is unlikely that CH_4 is migrating upwards from limestone, given that upward migration of CH_4 at sites over kimberlite is not supported by the redox conditions in kimberlite waters. The most likely source of CH_4 is the peat overlying the TSS, as drainage of peat groundwater could transport dissolved methane to the TSS. The reduction of DIC is generally considered the dominant pathway for the production of CH_4 in deeper peat zones (the catetolem) (Lansdown et al., 1992; Hornibrook et al., 2000; Beer and Blodau, 2007). This pathway is consistent with the methane samples in this study, as between 80 and 100% of the CH_4 (regardless of whether the samples were collected over kimberlite or limestone) has been derived from the groundwaters in which DIC reduction is taking place (Fig. 7).

6. Summary and conclusions

In summary, buried kimberlites likely influence the redox environment in TSS overlying kimberlites, which results in changes in the CO_2–CH_4 system in the TSS groundwater. The schematic diagram in Fig. 10 shows our interpretation of the CO_2–CH_4 system for groundwater in the TSS overlying kimberlite and limestone.

This study provides evidence that buried kimberlites from James Bay lowlands can alter the CO_2–CH_4 system in sediment overlying kimberlites. $\delta^{13}C_{DIC-CH4}$ values of approximately 72‰ coupled with increases in methane concentrations indicated CO_2 reduction for the majority of TSS groundwater samples over kimberlites. The same samples with $\delta^{13}C_{DIC-CH4}$ values of 72‰ are also those that plot along a Rayleigh fractionation curve for CO_2 reduction. Data suggest that methane in all but one sample was due to in situ methane formation. Common methane formation at these locations likely results from

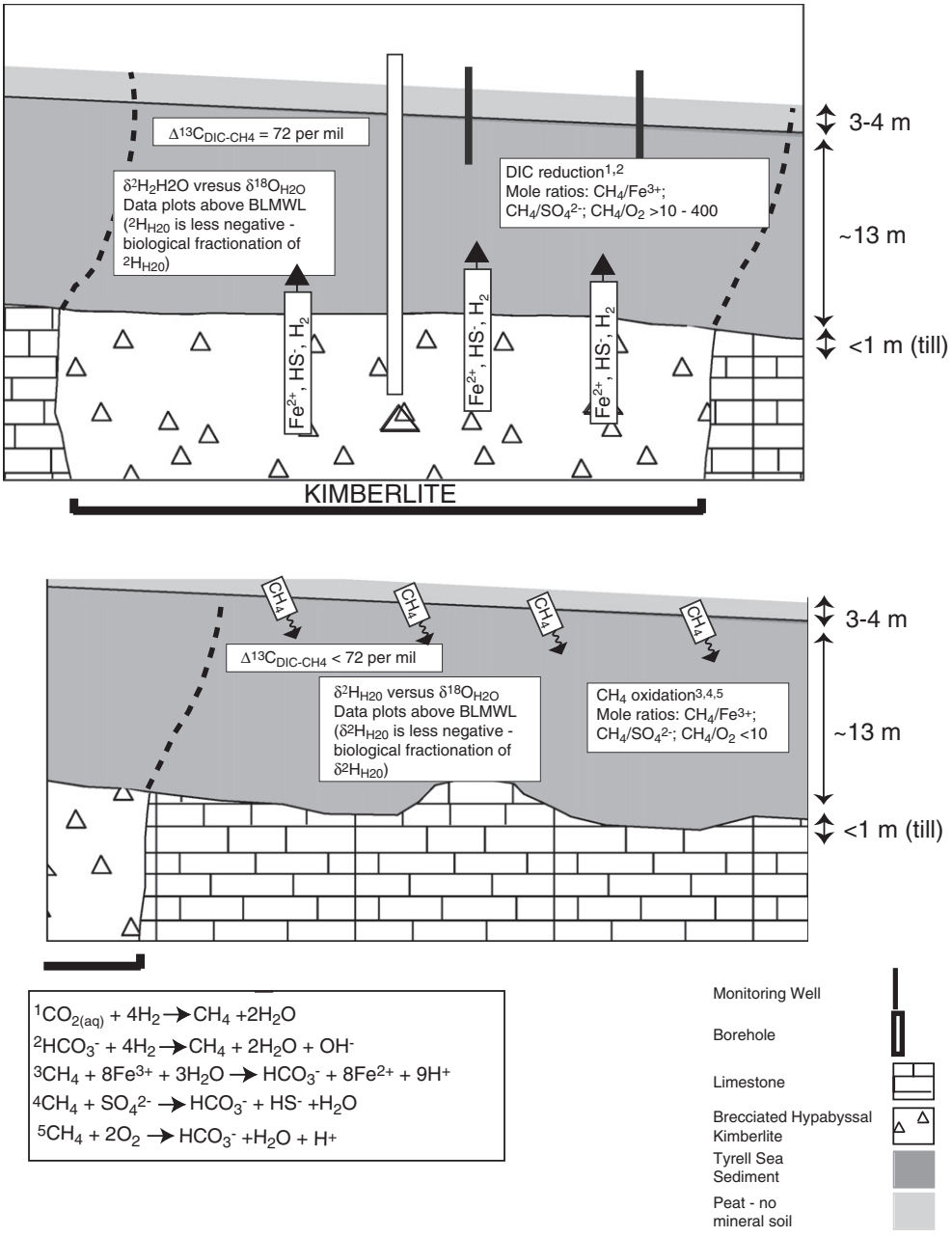

Fig. 10. Schematic cross-section of methane oxidation and DIC reduction pathways in the TSS over kimberlite (top) and limestone (bottom) in the Attawapiskat kimberlite field.

reduced ions in the underlying kimberlite groundwaters. Sites with low $\delta^{13}C_{DIC-CH4}$ values commonly had low CH_4/Fe^{3+}, CH_4/SO_4^{2-}, and $CH_4/O_{2(aq)}$ ratios.

Hydrocarbons have been used successfully to delineate buried kimberlites in the Ville-Marie region of western Quebec (Sader et al., 2009). McCarthy et al. (1986) indicated CH_4 anomalies near surface were associated with a buried sulfide deposit. Additionally, a number of commercial laboratory packages exist to delineate blind mineralization using reduced gas. However, the geochemical processes that are producing the gas anomalies are not fully understood. The results of this study have implications for geochemical exploration and the origin of reduced gas anomalies over mineralization. The use of isotopes and CH_4 gas concentrations, coupled with isotopic values of DIC in groundwaters over Attawapiskat kimberlites provides further insight into processes that are responsible for these gas anomalies. Our work suggests that methane anomalies over kimberlites are related to in situ formation within the TSS over the kimberlites, and not directly due to water–kimberlite reactions.

Further research into mechanisms controlling the DIC–CH_4 system over various rock types is required. The identification of redox and methane gradients by collecting groundwaters and gas samples systematically along vertical profiles within the TSS would provide additional information on the upward movement of redox sensitive ions and methane fluxes over kimberlites versus outside of them. Additionally, the collection of methane in peat over and outside kimberlites would provide more information on the methane formation or oxidation in peat groundwaters.

Acknowledgments

We thank DeBeers Canada for providing financial and logistical support for the project. Julie Kong, Ed Francisco, and Brad Wood were particularly helpful. Financial support was also provided by a NSERC Discovery grant and a NSERC Collaborative Research grant to Keiko Hattori. Jamil Sader received financial support from an Ontario Graduate Scholarship and a student research grant from the Society of Economic Geologists. A scholarship awarded to Jamil from the G.G. Hatch Laboratory (University of Ottawa) covered partial isotope analytical costs. Fieldwork was assisted by Katherine Mellor. We thank M. Beth McClenaghan (Geological Survey of Canada) and Matthew Leybourne (ALS Geochemistry) for input and assistance in writing the paper. We thank Chemical Geology Editor-in-Chief David Hilton and an anonymous reviewer for comments that greatly improved the manuscript.

References

Abrajano, T.A., et al., 1988. Methane–hydrogen gas seeps, Zambales ophiolite, Philippines: deep or shallow origin? Chem. Geol. 71, 211–222.
Achtnich, C., Bak, F., Conrad, R., 1995. Competition for electron donors among nitrate reducers, ferric iron reducers, sulfate reducers, and methanogens in anoxic paddy soil. Biol. Fertil. Soils 19 (1), 65–72.
Armstrong, J.P., Wilson, M., Barnett, R.L., Nowicki, T., Kjarsgaard, B.A., 2004. Mineralogy of primary carbonate-bearing hypabyssal kimberlite, Lac de Gras, Slave Province, Northwest Territories, Canada. Lithos 76, 415–433.
Barnes, I., Rapp, J.B., O'Neil, J.R., 1972. Metamorphic assemblages and the direction of flow of metamorphic fluids in four instances of serpentinization. Contrib. Mineral. Petrol. 35, 263–270.
Beer, J., Blodau, C., 2007. Transport and thermodynamics constrain belowground carbon turnover in a northern peatland. Geochim. Cosmochim. Acta 71, 2989–3002.
Bellefleur, G., et al., 2005. Downhole seismic imaging of the Victor Kimberlite, James Bay Lowlands, Ontario; a feasibility study. Open File Report 2005-C1, Geological Survey of Canada, p. 7.
Bethke, C.M., 2002. The Geochemist's Workbench — Release 4.0. University of Illinois.
Birks, S.J., et al., 2003. Canadian Network for Isotopes in Precipitation. University of Waterloo/Meteorological Service of Canada, Waterloo, Ontario.
Bottinga, Y., 1969. Calculated fractionation factors for carbon and hydrogen isotope exchange in the system calcite–carbon dioxide–graphite–methane–hydrogen–water vapor. Geochim. Cosmochim. Acta 33 (1), 49–64.
Brauneder, K., 2007. Characterization of peatland waters overlying concealed kimberlites in the Attawapiskat region, northern Ontario. B.Sc. Hon. Thesis University of Ottawa, Ottawa (76 pp.).
Cameron, E.M., Hamilton, S.M., Leybourne, M.I., Hall, G.E.M., McClenaghan, M.B., 2004. Finding deeply buried deposits using geochemistry. Geochem. Explor. Environ. Anal. 4 (1), 7–32.
Clark, I.D., Fritz, P., 1997. Environmental Isotopes in Hydrogeology. Lewis Publishers, Boca Raton, New York (328 pp.).
Clymo, R.S., 1984. The limits to peat bog growth. Philos. Trans. R. Soc. Lond. B Biol. Sci. 303 (1117), 605–654.
Fritz, P., Clark, I.D., Fontes, J.-C., Whiticar, M.J., Faber, E., 1992. Deuterium and (super 13) C evidence for low temperature production of hydrogen and methane in a highly alkaline groundwater environment in Oman. In: Kharaka, Y.K., Maest, A.S. (Eds.), Proceedings — International Symposium on Water–Rock Interaction, vol.7, pp. 793–796.
Hamilton, S.M., Hattori, K.H., Clark, I.D., 2005. Investigation into the source of forest-ring related natural gas in northern Ontario. Open File Report, 6172. Ontario Geol. Survey, pp. 19-1–19-4.
Hansen, L.K., Jakobsen, R., Postma, D., 2001. Methanogenesis in a shallow sandy aquifer, Romo, Denmark. Geochim. Cosmochim. Acta 65 (17), 2925–2935.
Heilweil, V.M., Solomon, K.D., Perkins, K.S., Ellett, K.M., 2004. Gas-partitioning tracer test to quantify trapped gas during recharge. Ground Water 42 (4), 589–600.
Hornibrook, E.R.C., Longstaffe, F.J., Fyfe, W.S., 2000. Evolution of stable carbon isotope compositions for methane and carbon dioxide in freshwater wetlands and other anaerobic environments. Geochim. Cosmochim. Acta 64 (6), 1013–1027.
Jakobsen, R., Postma, D., 1999. Redox zoning, rates of sulfate reduction and interactions with Fe-reduction and methanogenesis in a shallow sandy aquifer, Rømø, Denmark. Geochim. Cosmochim. Acta 63, 137–151.
Jakobsen, R., et al., 1998. H_2 concentrations in a landfill leachate plume (Grindsted, Denmark): in situ energetics of terminal electron acceptor processes. Environ. Sci. Technol. 32 (14), 2142–2148.
Kong, J.M., Boucher, D.R., Scott Smith, B.H., 1999. Exploration and geology of the Attawapiskat Kimberlites, James Bay Lowland, northern Ontario, Canada. In: Gurney, J.J., Gurney, J.L., Pascoe, M.D., Richardson, S.H. (Eds.), Proceedings of the International Kimberlite Conference, pp. 452–467.
Kumaraswamy, S., Ramakrishnan, B., Sethunathan, N., 2001. Methane production and oxidation in an anoxic rice soil as influenced by inorganic redox species. J. Environ. Qual. 30 (6), 2195–2201.
Lansdown, J.M., Quay, P.D., King, S.L., 1992. CH (sub 4) production via CO (sub 2) reduction in a temperate bog; a source of (super 13) C-depleted CH (sub 4). Geochim. Cosmochim. Acta 56 (9), 3493–3503.
Lovell, J.S., Hale, M., Webb, J.S., Parslow, G.R., 1983. Soil air carbon dioxide and oxygen measurements as a guide to concealed mineralizations in semi-arid and arid regions. J. Geochem. Explor. 305–317.
Manning, A.H., Solomon, K.D., 2003. Using noble gases to investigate mountain-front recharge. Journal of Hydrology 275, 194–207.
Martens, C.S., Berner, R.A., 1977. Interstitial water chemistry of anoxic Long Island Sound sediments; 1, dissolved gases. Limnol. Oceanogr. 22 (1), 10–25.
McCarthy Jr., J.H., Lambe, R.N., Dietrich, J.A., 1986. A case study of soil gases as an exploration guide in glaciated terrain; crandon massive sulfide deposit, Wisconsin. Econ. Geol. Bull. Soc. Econ. Geol. 81 (2), 408–420.
Miura, Y., Watanabe, A., Murase, J., Kimura, M., 1992. Methane production and its fate in paddy fields II. Oxidation of methane and its coupled ferric oxide reduction in subsoil. J. Plant Nutr. Soil Sci. 38 (4), 673–679.
Norris, A.W., 1993. Hudson Platform; introduction. In: Stott, D.F., Aitken, J.D. (Eds.), Sedimentary Cover of the Craton in Canada. Geol. Surv. Canada, Ottawa.
Proskurowski, G., et al., 2008. Abiogenic hydrocarbon production at Lost City hydrothermal field. Science 319 (5863), 604–607.
Reeve, A.S., Siegel, D.I., Glaser, P.H., 1996. Geochemical controls on peatland pore water from the Hudson Bay Lowland; a multivariate statistical approach. J. Hydrol. 181 (1–4), 285–304.
Rejmankova, E., Post, R., 1996. Methane in sulfate-rich and sulfate-poor wetland sediments. Biogeochemistry 34 (2), 57–70.
Sader, J.A., Leybourne, M.I., McClenaghan, M.B., Hamilton, S.M., 2007a. Low-temperature serpentinization processes and kimberlite ground water signatures in the Kirkland Lake and Lake Timiskiming kimberlite fields, Ontario, Canada; implications for diamond exploration. Geochem. Explor. Environ. Anal. 7 (1), 3–21.
Sader, J.A., Leybourne, M.I., Mclenaghan, M.B., Clark, I.D., Hamilton, S.M., 2007b. Antacid belches from northeastern Ontario: generation of high pH groundwaters and H2 gas. International Applied Geochemical Symposium, Ovideo, Spain, June 14–19, 2007.
Sader, J.A., Anderson, H.S.I., Fenstermacher, R.F., Hattori, K.H., 2009. Imaging a buried diamondiferous kimberlite using conventional geochemistry and amplified geochemical imaging technology. In: Lentz, D.R., Thorne, K.G., Beal, K. (Eds.), 24th International Applied Geochemistry Symposium. Association of Applied Geochemists, Fredericton, NB, Canada.
Sader, J.A., Hattori, K.H., Kong, J.M., Hamilton, S.M., 2011. Geochemical responses in peat groundwater over Attawapiskat kimberlites, James Bay Lowlands, Canada and their application to diamond exploration. Geochem. Explor. Environ. Anal. 11, 193–210.
Sage, R.P., 2000. Kimberlites of the Attawapiskat Area, James Bay Lowlands, Northern Ontario. Open File Report, 6019. Ontario Geological Survey, p. 341.
Sanford, W.E., Shropshire, R.G., Solomon, K.D., 1996. Dissolved gas tracers in groundwater: simplified injection, sampling, and analysis. Water Resour. Res. 32 (6), 1635–1642.
Schoell, M., 1980. The hydrogen and carbon isotopic composition of methane from natural gases of various origins. Geochim. Cosmochim. Acta 44 (5), 649–662.
Segers, R., 1988. Methane production and methane consumption: a review of processes underlying wetland methane fluxes. Biogeochemistry 41, 23–51.

Sheldon, A., 2002. Diffusion of Radiogenic Helium in Shallow Ground Water: Implications for Crustal Degassing. Ph.D. dissertation University of Utah, Department of Geology and Geophysics, Salt Lake City, Utah.

Shilts, W.W., 1986. Glaciation of the Hudson Bay Region. In: Martini, I.P. (Ed.), Canadian Inland Seas. Elsevier Science Publishers B.V., Amsterdam, The Netherlands, p. 494.

Siegel, D.I., Chanton, J.P., Glaser, P.H., Chasar, L.S., Rosenberry, D.O., 2001. Estimating methane production rates in bogs and landfills by deuterium enrichment of pore water. Global Biogeochem. Cycles 15 (4), 967–975.

van Straaten, B.I., Kopylova, M.G., Russell, J.K., Webb, K.J., Smith, B.H.S., 2009. Stratigraphy of the intra-crater volcaniclastic deposits of the Victor Northwest kimberlite, northern Ontario, Canada. Lithos 112 (Supplement 1), 488–500.

Webb, K.J., Scott Smith, B.H., Paul, J.L., Hetman, C.M., 2004. Geology of the Victor Kimberlite, Attawapiskat, northern Ontario, Canada; cross-cutting and nested craters. Lithos 76, 29–50.

Whiticar, M.J., 1999. Carbon and hydrogen isotope systematics of bacterial formation and oxidation of methane. Chem. Geol. 161 (1–3), 291–314.

Whiticar, M.J., Faber, E., 1986. Methane oxidation in sediment and water column environments; isotope evidence. Org. Geochem. 10, 759–768.

Whiticar, M.J., Faber, E., Schoell, M., 1986. Biogenic methane formation in marine and freshwater environments; CO (sub 2) reduction vs. acetate fermentation; isotope evidence. Geochim. Cosmochim. Acta 50 (5), 693–709.

Yu, K., Bohme, F., Rinklebe, J., Neue, H.-U., DeLaune, R.D., 2007. Major biogeochemical processes in soils — a microcosm incubation from reducing to oxidizing conditions. Soil Sci. Soc. Am. J. 71 (4), 1406–1417.